EUROPEAN ORGANIZATION FOR NUCLEAR RESEARCH
European Laboratory for Particle Physics

CERN - SL DIVISION

CERN/SL/93-26 (EA)

THE UPGRADED MUON BEAM AT THE SPS

N. Doble, L. Gatignon,
G. von Holtey, F. Novoskoltsev [a)]

ABSTRACT

The SPS muon beam, recently upgraded for the Spin Muon Collaboration experiment, is described. The basic concepts of the beam design are presented. The measured beam flux and muon halo rates, spot sizes and average muon polarisation are reported and the observed performance is compared with Monte Carlo simulations.

(Submitted to Nuclear Instruments and Methods A)

Geneva, 16 June, 1993

a) Now at Institute for High-Energy Physics, Protvino, Russia

CONTENTS

1. INTRODUCTION

This paper describes the high-energy muon beam at the Super Proton Synchrotron at CERN. The first implementation of the muon beam dates back to 1978 [1]. At the beginning of 1991 the beam was upgraded to match the needs of the Spin Muon Collaboration, which is carrying out a precision measurement of spin-dependent nucleon structure functions [2]. We present the concept, layout and performance of the present SPS muon beam. In section 2 we discuss the requirements and boundary conditions. In section 3 we explain the basic concept and the beam optics. In section 4 we give the results of Monte Carlo simulations of the beam line. Section 5 discusses the special equipment and instrumentation installed. In section 6 we report on the observations and measurements of the beam parameters and compare the performance with Monte Carlo predictions. Summary and conclusions are given in section 7.

2. REQUIREMENTS FOR THE SPS MUON BEAM

The M2 muon beam was commissioned in 1978 to serve the EMC [3] and BCDMS [4] experiments and was subsequently used by the NMC experiment [5]. Finally, from 1991 onward, the beam is being used by the Spin Muon Collaboration.

Originally the muon beam was designed to transport high fluxes of muons of the maximum feasible momenta, up to 325 GeV/c, that could be derived from a primary proton beam of 400/450 GeV/c. The rate required by the experiments was $\approx 10^8$ and $\approx 10^7$ μ^+ per SPS pulse at beam momenta of 200 and 280 GeV/c, respectively. In the experimental hall EHN2 two experiments were installed in series and the beam was normally focused on the upstream one. The waist was such that, after slight refocusing in the vertical plane, the beam size remained tolerable for the downstream experiment. Nowadays only one experiment is installed in the same experimental hall, but it comprises two relatively independent sections, used simultaneously and occupying the full length ($\approx$ 110 metres) of the hall. The emphasis has turned to a high degree of longitudinal polarisation, rather than maximum rate or momentum.

Based on the new requirements of the Spin Muon Collaboration for the measurement of the spin dependence of the nucleon structure functions, we derive the following conditions on the performance of the SPS muon beam :

1) The momentum range of the muons delivered to the experimental hall should be in the range between 100 and 225 GeV/c. The energy of the primary proton beam, extracted from the SPS, is 450 GeV/c.
2) At the nominal beam energy of 100 GeV/c, the maximum flux per 2.56 seconds long SPS pulse should be well above $5 \cdot 10^7$ muons for reasonable extracted proton beam intensities, not exceeding 10^{13} protons per pulse. The SPS repetition rate is normally 14.4 seconds.
3) To allow an average longitudinal polarisation of at least 80%, the momentum band of the muons transported to the experimental hall should not exceed $\Delta p/p = \pm 5\%$. For the same reason the momentum band selected for the parent particles should not exceed $\Delta p/p = \pm 10\%$.
4) There should be a beam stage allowing for particle-by-particle momentum measurement of the muons with a relative precision of $\Delta p/p_0$ (measured) better than $\pm 1\%$.
5) The hadron contamination in the muon beam should be negligible, i.e. below a level of $\pi / \mu \leq 10^{-6}$.
6) The beam should be contained within a diameter of 50 mm at the polarised target, located some 17 metres downstream of the entrance to the experimental hall.
7) The polarised target is followed by a $\approx$ 30 metres long spectrometer, which is in turn followed by a polarimetry section comprising a muon decay length, a 6 metres long spectrometer magnet, MNP26, and a system of wire chambers and electromagnetic calorimeter at the end of the hall. The distance between the centre of MNP26 and the polarised target is approximately 75 metres. The decay length should be at least 30 metres long. The vertical beam spot at MNP26 should not exceed the 140 mm magnet gap, whilst horizontally the r.m.s. size of the beam should be smaller than 25 mm to allow for an adequate acceptance of the polarimeter.
8) The beam should be nearly dispersion free in momentum at the experimental hall so as to yield a sufficiently small beam spot all along the hall.
9) The halo of unwanted muons reaching the experimental apparatus in a surface of 4x4 m^2, outside the beam radius of e.g. 10 cm, should be reduced to $\leq$ few 10^6 μ/pulse.

3. CONCEPTS AND OPTICS

To meet the above requirements, the beam design has been based on two independent sections, a hadron acceptance and decay channel 600 m in length (of order 10% of the pion decay length at 100 GeV/c), to obtain an appreciable muon yield, followed by a muon transport section that serves to select and clean the muon beam produced upstream and to transport and focus it to the experiment.

The layout of the SPS muon beam, with indications of its basic functions, is shown in figure 1. The basic functions of the different sections are described below and the main parameters are listed whenever appropriate.

3.1 Hadron section of the beam

The 450 GeV/c primary proton beam with intensity between 10^{12} and 10^{13} protons per SPS pulse, impinges on a primary target made of 2 or 3 mm thick Beryllium plates. The target is equipped with secondary emission monitors to permit fine steering of the proton beam to within $\approx \pm 0.1$ mm in each plane [6]. A number of different target lengths is available, but for normal operation 30 or 50 cm long plates are used to yield the maximum outgoing hadron flux. The plates are air-cooled to allow proton fluxes of up to 10^{13} protons per SPS pulse. Shorter target plates are provided for low-intensity calibration runs. The target efficiency, i.e. the yield of useful secondary pions, can be calculated as the product of the probability to have a primary interaction in the target and the probability that the secondary particles produced are not absorbed within the target. This leads to a target efficiency ε_t that depends on the target length L as

$$\varepsilon_t(L) = \frac{e^{-L/\lambda_\pi}}{1-\lambda_p/\lambda_\pi}\left\{1 - e^{-(L/\lambda_p)\,(1-\lambda_p/\lambda_\pi)}\right\}$$

with $\lambda_p = 43.5$ cm and $\lambda_\pi = 60$ cm [7,8]. This dependence is shown in figure 2.

The optics for the transport of the secondary charged particles produced in the primary target is shown in figure 3. It is seen that the target is immediately followed by a series of 6 quadrupoles (Q1 – Q6), used at high gradients to provide maximum acceptance for the charged particles emerging around 0 mrad production angle from the target. These quadrupoles are followed by a first set of horizontal dipole magnets (B1), that provides the dispersion necessary for momentum selection of the parent pions and kaons. The primary protons that traversed the target without

interaction are deflected in a different direction and may be recuperated and transported by the neighbouring P61/62 beam line towards the high-intensity underground area. In case the latter beam is required, the momentum of the parent hadrons in the muon beam is constrained to be –225 GeV/c for the P61/P62 momentum of +450 GeV/c. Otherwise the momentum of the parent hadrons can be chosen freely in the range below ± 300 GeV/c.

After the first momentum defining bend, unwanted particles are dumped in a massive, 3.2 metres long pair of dump collimators, called TAX 1+2. These dump collimators are motorised and allow the hadron beam to be completely absorbed in case of access to the experimental area. The momentum band is selected with a set of two adjustable collimators, C1 and C3, placed some 25 m downstream of the momentum defining bend. At the location of these collimators (opening range ± 57 mm) the dispersion is 5 mm per %, allowing a maximum momentum bite of approximately ± 10%. The vertical collimators C2 and C4 can be used to reduce the acceptance of the beam. The collimators straddle a small vertical bend (B2) and are followed, after refocusing the off-momenta, by a second horizontal dipole (B3), necessary to compensate for the horizontal dispersion introduced by B1. Five more quadrupoles (Q7 – Q11) serve to achieve full dispersion recombination and to provide matching into the hadron decay channel. The decay channel itself (Q12 – Q18) is composed of a regular structure of alternately focusing and defocusing, large aperture (200 mm diameter) quadrupoles. Fifteen 2 metre-long quadrupoles, placed at 36 metre intervals, provide a ≈ 500 metre-long so-called FODO-structure, more commonly used in accelerators, that transports both the parent hadrons and the lower momentum decay muons with minimal losses. Each cell (a cell being defined as the length between successive quadrupoles of the same polarity) provides a 60° phase advance in each plane for the parent hadrons. In fact, as shown in figure 4, the acceptance of a symmetric FODO structure (with equal phase advance per cell in both planes) has a broad maximum around ≈ 70°/cell [9]). The 60° phase advance was chosen to keep good acceptance also for the decay muons, that have lower momentum (between ≈ 57% and 100% of the hadron momentum) and correspondingly larger phase advance per cell. At 110 GeV/c hadron momentum, about 10% of the pions decay and the beam at the end of the decay channel contains about 10% muons.

At the end of the decay channel three quadrupoles (Q19 – Q21) serve to focus the muons of the wanted momentum (and the parent hadrons) on to an absorber consisting of rods of Beryllium, embedded in Aluminium blocks, in which the remaining hadrons are stopped. The length of the absorber can be varied up to a total of 9.9 metres. The muons traverse the absorber with little energy loss (2–3 GeV), but undergo significant multiple Coulomb scattering in the absorber material. Note that Beryllium (small ratio of nuclear interaction length over radiation length) provides minimum multiple Coulomb scattering for a given hadron stopping power. The size of the waist at the absorber has been optimised for minimum effect of multiple Coulomb scattering over the full length of the absorber.

3.2 Muon section of the beam

The muon section of the beam starts at the hadron absorber. The optics of this section is shown in detail in figure 5. The length of the decay channel was maximised by installing the absorber as far downstream as possible, inside the first vertical bend (B4) of the muon section of the beam. Thereby momentum dispersion and scattering of the muons occur in this element. The presence of a waist in the first bend of the muon section (B4+B5, total angle 24.0 mrad), however, minimises the effect of the multiple Coulomb scattering in the Beryllium absorber (up to 28 radiation lengths).

The muon beam is bent back to the horizontal plane by Bend-6. Dispersion compensation in angle at the exit of Bend 6 is obtained if the relation $\theta_1 + m_{46} \cdot \theta_2 = 0$ holds [7], where m_{46} is the magnification of the waist in B6 with respect to that in B4+5, and θ_1, θ_2 are the bending angles of B4+5 and B6, respectively. In the muon beam, total dispersion compensation is achieved by point-to-point imaging from the waist in the first bend (24 mrad) to the second bend (33.69 mrad) with magnification $24.0/33.69 \approx 0.712$ as required by the above relation.

Some 40 metres downstream of the first bend, a system of two 5 metre-long vertical magnetic collimators or 'scrapers' (SCRAPER 4 and 5) allows the muon momentum band to be defined. The dispersion at the position of these collimators increases from 8 mm/% at the entrance of SCRAPER 4 to 13 mm/% at the exit of SCRAPER 5. These collimators provide a ≈ 1.5 Tesla toroïdal field in the iron around the beam, whilst producing only a negligible quadrupolar stray field inside the beam aperture. The two jaws have independent motors at each end, so that the gap can be adjusted to match the beam profile through the collimator.

The momentum-selected muon beam emerging from the absorber and scrapers is matched (Q22 – Q24) into a second 3 cells long FODO structure (Q25 – Q27), again with 60° phase advance per cell. The focusing section (Q28 – Q30) into the second and final vertical bend (B6) is similar to, but shorter than the matching section downstream of B5. To achieve this shortening while respecting an existing tunnel layout, the second half of the FODO structure had to be stretched (lattice spacing 44.8 metres, to be compared to 36 metres in the first half). The appropriate size of the waist at B6 (for dispersion recombination) is in fact obtained by choosing a length of the matching section 0.712 x (44.8/36.0) times shorter than the matching section following B5, where 0.712 is the ratio of the bending angles in B4+5 and B6.

The second vertical bend B6 is used to form the 'Beam Momentum Station'. It is surrounded symmetrically by two pairs of quadrupoles (Q29 and Q30) and in particular also two pairs of scintillator hodoscopes (HODO 1 – 4) that allow a precise measurement of the position and hence the momentum of individual muons [10] (see section 5).

The section between the absorber and B6 also serves to remove unwanted halo muons. Seven magnetic collimators (2 horizontal and 5 vertical) and two magnetic shielding blocks (MIBs) remove the so-called halo of muons surrounding the core of the beam. Since each magnetic collimator gives a lateral momentum kick of approximately 2 GeV/c, corresponding to $\approx$ 10 milliradians at the higher muon energies, several hundred metres of distance are needed to reduce effectively the muon halo in a $\geq 4 \times 4$ m^2 area at the experiment.

The final section of the beam (Q31 – Q35) contains the optics necessary to provide adequate beam spot sizes at the various parts of the experiment. In the experimental hall, the 6 milliradians bend of the experimental spectrometer magnet (B8) is compensated (almost symmetrically) by two horizontal bends of $\approx$ 3 mrad each (B7 and B9). Downstream of B9 a 30 metres decay length, followed by a spectrometer magnet (B10) and a multitude of detectors, serves to measure the average polarisation of the muons in the beam. See figure 6 for a schematic layout of the experimental hall.

3.3 Longitudinal polarisation

One motivation for the new muon experiment is the study of the spin-dependence of the nucleon structure functions. Hence the need of a polarised beam and a polarised target. Longitudinal polarisation of the muons occurs naturally due to parity violation in the $\pi \rightarrow \mu\ \nu_\mu$decay [11]. For each charged pion or kaon decay into a muon and neutrino, the helicity h is related to the centre-of-mass decay angle θ^* of the muon with respect to the pion direction in the laboratory frame by

$$h = \frac{E^* \cos\theta^* + p^*}{E^* + p^* \cos\theta^*}$$

where p* and E* refer to the momentum and energy of the muon in the pion rest frame. This relation is plotted in figure 7. The longitudinal beam polarisation p_L is the average helicity in the laboratory frame, integrated over the beam phase space. Maximum longitudinal polarisation (in absolute value) is obtained in the limits $\cos\theta^* \rightarrow \pm 1$, corresponding to muon momentum close to 57% ($\cos\theta^* \approx -1$) or 100% ($\cos\theta^* \approx +1$) of the parent pion momentum. In figure 8 the polarisation is plotted against p_μ/p_{hadron} both for pion and kaon decays, again for monochromatic pencil beams. Note that for muons from forward kaon decay ($\cos\theta^* \rightarrow +1$), present in the beam at levels up to a few percent, the polarisation is even higher than for muons from pion decay. However, at 57% of the hadron energy, where $\cos\theta^* \approx -1$ for muons from pion decay, $\cos\theta^*$ is still positive in the case of kaon decays. Therefore at p_μ/p_{hadron} close to 0.57 the average muon polarisation will be degraded by any presence of muons from kaon decay. One also sees from the slope of the pion curve in figure 8 that a maximum degree of muon polarisation is anyway more easily obtained for p_μ/p_{hadron} close to 1, even ignoring the muons from kaon decay.

Also the muon intensity is a strong function of $\cos\theta^*$. In the extreme limits of phase space ($\cos\theta^* \rightarrow \pm 1$), the intensity drops to 0. Away from those limits, the intensity increases rapidly with a maximum at $p_\mu/p_{hadron} \approx 0.9$ (see below). The choice for p_μ/p_{hadron} will be a compromise between high polarisation and high rate.

4. CALCULATIONS OF BEAM PERFORMANCE

The optics for the hadron section of the beam, starting at the primary target and ending with a waist at the absorber, was optimised to first and second order using the TRANSPORT charged particle transport optics program [12]. See figure 3 for the result. However, due to the large hadron momentum band transported, the results need to be verified by a Monte Carlo simulation. Such a simulation is also needed to calculate total beam flux per incident proton and to estimate the particle losses and resulting halo along the beam line. For the muon section of the beam, the calculations are complicated by the fact that the muons are not produced in a small and well defined target, but rather incoherently through pion and kaon decays along a 500 metre-long channel. In a first approximation the optics for the muon section was designed using the TRANSPORT program and assuming essentially a waist at the absorber position. Actually to take into account the dispersive effect of the vertical bend at the absorber position, we used as the starting point for the muon calculation another waist, 90^{o} upstream at the end of the hadron decay section. For the calculation and optimisation of the spot size at the experiment, we used an iterative approach, based on an effective phase space for the muons at the absorber, that was derived from Monte Carlo distributions by transport matrix inversion. During the commissioning of the beam, this procedure was even refined by using measured profiles rather than Monte Carlo distributions.

Using the fields and gradients obtained from the TRANSPORT runs, the beam was simulated in detail using the HALO Monte Carlo program[13]. This program simulates particle production in the primary target as well as pion (or kaon) decays along the decay channel. All particles are tracked through the elements of the beam line. Muons leaving the nominal aperture (called "halo" particles) are followed as well, taking into account field maps inside and outside the magnet yokes. Even the size of the tunnel and the thickness of the earth, concrete or iron shielding around the tunnel is taken into account. As at most a few percent ($\leq 3\%$) of the muons at the end of the beam line come from kaon decay, we have in most cases neglected the kaon component for the results given below.

The Monte Carlo simulation allows to calculate the beam spot sizes along the beam line, the beam flux, momentum band and halo levels around the beam as a function of magnetic fields and scraper and collimator positions. In fact the halo program was used to position the magnetic collimators suitably along the beam line. Also the average beam polarisation and beam flux (for open collimators in the

hadron section of the beam) were calculated as a function of the π/μ momentum ratio. For the case of 100 GeV/c muon momentum, the results are shown in figure 9. On the basis of these calculations a ratio of muon to hadron momenta between 0.90 and 0.92 was chosen as a suitable compromise between flux and polarisation. Based on this choice, we did extensive and more complete simulations for the cases ±110/100 GeV/c (where 110 denotes the central hadron momentum and 100 the central muon momentum in GeV/c) and ±225/208 GeV/c. The Monte Carlo predictions for these momenta are listed in table 1, assuming 10^{12} interacting (corresponding to $\approx 3.5\ 10^{12}$ incident) protons on the primary target. For these runs all (magnetic) collimators were wide open to allow for maximum muon flux.

The average polarisation of the beam depends somewhat on the momentum bands $\Delta p/p$, both in the hadron and muon sections of the beam. Therefore in reality the momentum slit of the hadron section of the beam was closed to ±4%. Under these conditions $3.5\ 10^{12}$ incident protons per pulse (of which $\approx 10^{12}$ effectively interact in the primary target) are required to achieve the nominal flux of $\approx 4 \cdot 10^7$ muons per SPS pulse at +100 GeV/c muon momentum, requested by the experiment. At –208 GeV/c the nominal flux cannot be achieved with such a limited momentum band, for the maximum proton intensity of 10^{13} protons per pulse, allowed on the primary target.

Hadron/μ energy (GeV/c)	+110/100	–110/100	+225/208	–225/208
Protons on target	35	35	35	35
Muons at experiment	10^8	$8\ 10^7$	$7\ 10^7$	$2.7\ 10^7$
RMS size at polarised target	14x13 mm	14x13 mm	12x15 mm	12x15 mm
RMS size at MNP26 entrance	16x20 mm	16x20 mm	17x20 mm	17x20 mm
Hadron momentum band	4%	4%	5%	5%
Muon momentum band	3.2%	3.2%	2.8%	2.8%
Near halo at polarised target	3%	3%	2%	2%
Far halo at polarised target	1%	1%	0.5%	0.5%
Near halo at MNP26	7%	7%	5%	5%
Far halo at MNP26	3%	3%	1%	1%

Table 1: Simulated beam performance with open collimators for high flux. The "near halo" is defined as the fraction of muons that arrive in a 50x50 cm^2 surface outside a 5 cm radius hole around the beam axis. The "far halo" is counted in a 4.0x4.0 m^2 surface outside a 50x50 cm^2 beam passage.

5. EQUIPMENT AND INSTRUMENTATION

In this section we give a short description of the special equipment used in the muon beam line. For more details we refer to the literature quoted.

5.1 Hadron absorber

The requirement of $\leq 10^{-6}$ hadron contamination in the muon beam leads to the need of sufficient material in the beam to absorb essentially all hadrons. As the average multiple scattering angle is proportional to the square root of the number of radiation lengths (which itself is approximately proportional to $1/Z^2$), it is important to choose a low-Z material [14]. We have chosen Beryllium rods, 55 mm in diameter, embedded in rectangular Aluminium blocks. The Aluminium should normally not be traversed by the muons. The complete absorber system consists of 9 modules, 1.1 metres long each. Therefore each module provides $\approx$ 2.7 interaction lengths, λ, of stopping power, whilst the number of radiation lengths per module is 3.1 X_0. Each of the modules is motorised independently, such that at lower hadron momenta up to 140 GeV/c only 7 modules are introduced into the beam, whereas at the higher momenta, where the multiple Coulomb scattering is suppressed by a factor $1/p$, the full stopping power of 9 modules is used. The modules are suspended in the three vertical bending magnets of B4, that each have a length of 3.0 metres and a gap width of 70 mm.

5.2 Scrapers and Magnetised Iron Blocks

Magnetic collimators (Scrapers) and Magnetised Iron Blocks (MIBs) are used to protect the experiment against unwanted halo particles outside the main beam. The basic concept relies on the use of small, but adjustable, magnetic collimators, followed by more massive, but static magnetised shielding blocks (MIBs) that enhance the deflection given by the scrapers.

A scraper is a system of four 5 metres long steel blocks, that are arranged to provide a toroïdal field around the beam. For the case of a horizontal scraper, illustrated schematically in figure 10, the left and right blocks are movable with two independent motors per block, one at the upstream and one at the downstream end. The other two blocks form fixed yokes, which are surrounded by coils that provide an adjustable toroïdal field ($\leq$ 1.5 Tesla) inside the iron. The quadrupolar stray field inside the beam tube is sufficiently small not to perturb the beam properties in any

noticeable way. The size of the coils limits the gap size to a minimum of ± 25 mm about the beam axis. The maximum gap size is ± 100 mm, equal to the aperture of the quadrupoles in the FODO channels. All four motors of each scraper have separate remote control. This allows the scraper positions to be optimised according to the beam profile and flux and halo requirements. Nevertheless the procedure is iterative and therefore lengthy due to correlations between the gaps of different scrapers.

The MIBs are more massive objects without motors. They are constructed in 1.6 metre-long modules, tailored to the requirements of the beam. In the muon beam their outside shape is square with outer dimension ≈ 1.6 x 1.6 m^2. The inner hole is ≈ 21 x 21 cm^2 to allow a 20 cm diameter beam tube to pass through easily. The field strength inside the iron is again about 1.5 Tesla. The quadrupolar stray field inside the beam tube is negligible.

One vertical scraper (SCRAPER 1, see figure 3) is installed just upstream of the absorber to reduce the halo of muons produced in the hadron section of the beam. Almost immediately following the absorber a system of two horizontal and three vertical collimators (SCRAPERs 2 - 6), followed by 8 metres of MIBs, perform the main cleaning of the muon beam. Two of the vertical scrapers also serve as momentum slit. The final cleaning of the beam is assured by a vertical scraper (SCRAPER 7) and a MIB, downstream of the last vertical bend (B6) and just before the entrance to the experimental hall. See figure 5.

5.3 Standard Beam Monitoring

The steering of the proton beam onto the primary target is monitored by various sets of secondary emission monitors, in particular split foil counters upstream and downstream of the target heads. The position of the incident beam can be controlled to within ± 0.1 mm.

Along the beam line 10 multiwire proportional chambers each with horizontal and vertical planes are installed [15]. Their wires can be grouped depending on the expected beam spot size so their effective spacing can be varied between 2 and 6 millimetres. Their analogue readout allows not only to obtain beam profiles, but also a relative measure of the beam intensity [16]. Four chambers (MWPC 1-8) are installed in the hadron section of the beam. They are provided with an in–out movement, to restrict the time during which they suffer radiation

damage. One chamber is located just downstream of the absorber (MWPC 9+10). Two more chambers (MWPC 11-14) allow the position of the beam at the entrance and exit of the beam momentum station to be measured. The remaining chambers are located close to the polarised target and at the beginning and end of the polarimeter decay section. See figures 3 and 5.

The beam and halo intensities are precisely monitored by various detectors belonging to the Spin Muon Collaboration. Some of the signals are read into scalers attached to the SPS Experimental Area control system.

In addition two ionisation chambers have been installed, that provide a measurement of the beam intensity to ±1%. One chamber is installed 10 metres upstream of the hadron absorber to record the flux in the hadron section of the beam. The second one is installed in the experimental hall, at the beginning of the polarimeter section. It records the muon flux provided to the experiment.

5.4 The Beam Momentum Station

The Beam Momentum Station (BMS) consists of four scintillator hodoscopes, located symmetrically around the final vertical bend [10]. The schematic layout of this section is shown in figure 11. Each module consists of 64 horizontal Pilot-U scintillator fingers, each read out through a Plexiglas 218 light guide by a fast 9826B photo-multiplier with Bialkali photo cathode. Each finger has a width of 5 mm and 20 mm thickness along the beam. As shown in figure 12, the length of the fingers in the horizontal plane has been adapted to the local beam intensity in order to limit the rate per photo multiplier to $3 \cdot 10^7$ particles per SPS pulse. The system has been designed to measure the momentum of more than 10^8 individual particles per burst with a relative precision of 1%. In order to eliminate ambiguities in the reconstruction of particle trajectories, their time of transit is measured with a resolution of 50 psec. A multi-user readout system allows simultaneous measurement of the beam momentum by the experiment and tuning or tests of the instrument by the SPS experimental area staff.

The relative momentum measurement depends mainly on geometry, beam optics in between the four modules and scintillator spacing. These parameters lead to a precision of ± 1%. The absolute momentum measurement depends also on misalignment of the BMS modules and the quadrupoles in between, knowledge of the field integral of the momentum defining dipole magnet versus current and on

the current delivered by the power supply. One way to measure the absolute momentum scale is to calibrate against an independent spectrometer in the experiment, which may be known to better precision, but need not have the rate capability of the Beam Momentum Station.

6. OBSERVED BEAM PERFORMANCE

In its present form the beam was put into operation early in 1991. Since then operational experience has been acquired at two different muon energies, namely 100 and 208 GeV/c. The parent hadron momentum was 110 and 225 GeV/c, respectively. Both positive and negative beams have been provided. The ratio of muon and hadron momenta ($p_\mu/p_\pi \approx 0.92$) has been chosen as a reasonable compromise between muon intensity and average longitudinal polarisation of the beam (see Section 4). The majority of the data taking has been at +100 GeV/c μ^+ momentum. In table 2 we list the observed muon beam and halo flux per SPS pulse under these conditions for the typical proton flux on the primary target [17,18]. For comparison the Halo Monte Carlo results are also shown. The Monte Carlo results are slightly different from the ones given in section 4, as we have here taken into account the beam settings and counter characteristics actually used during SMC data-taking.

Beam momentum (hadron →muon)	+ 110 → + 100 GeV/c	
	Data	Halo MC
Proton intensity (incident) on target per pulse	≈3.5 10^{12}	
Muon intensity per pulse in R = 5 cm	$4 \cdot 10^7$	$3 \cdot 10^7$
RMS beam size at polarised target (mm x mm)	16 x 15	13 x 13
RMS beam size at the polarimeter (mm x mm)	23 x 23	19 x 22
Momentum spread of hadrons (RMS_p/p)	not measured	≈ 5%
Momentum spread of muons (RMS_p/p)	3.6 %	3.3 %
Average longitudinal polarisation	(–82±6) %	(–83 ± 5) %
Fraction of un-vetoed beam	≈ 57 %	(59 ± 2) %
Hard halo	6 %	(4.5 ± 1) %

Table 2 : Observed beam performance in comparison with HALO Monte Carlo predictions

Actually two halo rates are presented. The so-called "veto rate" is the "Or" of six veto counters. In table 3 we give their longitudinal positions with respect to the polarised target centre and the approximate sizes of the counters. This veto rate measures the halo over a large surface, while leaving only a small hole for the beam passage. In fact, due to this small hole an appreciable fraction of the Gaussian tails (beyond $\approx 2\,\sigma$) of the beam are vetoed. The "hard halo" is the halo rate far away from the beam axis. It is measured over a surface of approximately 4x4 m^2 with an approximately square hole of ≈ 0.5x0.5 m^2. In general the agreement is surprisingly good. The largest disagreement (25%) is found for the muon flux. Various experimental uncertainties may have played a role in this, e.g. the limited knowledge of the proton flux.

Counter	Longitudinal position (m)	Total size H x V (m2)	Hole size (mm)	Comments
V1	–23.20	0.45 x 0.45	75 x 120	
V1.e	–31.13	0.11 x 0.11	—	4.5 cm below the beam
V1.5	–11.86	0.50 x 0.50	130 mm Ø	
V2	–3.10	0.41 x 0.41	70 mm Ø	
V2.1	–9.61	0.30 x 0.30	80 mm Ø	
V3	–10.88	5.00 x 2.00	500 x 500	

Table 3: The positions and dimensions of the counters used in the veto rate measurement.

In table 2 we have also indicated the longitudinal muon polarisation as measured recently by the SMC experiment [18,19]. The measured value, -0.82 ± 0.06, is in excellent agreement with the Monte Carlo simulation, that gave -0.83 ± 0.05. Note that in this case the Monte Carlo calculation includes a small correction for the fact that at this beam momentum $\approx 3\%$ of the muons come from kaon decays. The quoted error on the Monte Carlo is dominated by systematic uncertainties, in particular reasonable guesses for deviations in the central values and spreads of the hadron and muon momenta in the presence of misalignments and missteering of the beam.

In figures 13 and 14 we show the observed beam profiles at the polarised target and at the entrance to MNP26, respectively. They are compared to the Monte Carlo predictions. Both at the target and at the polarimeter the agreement is satisfactory. The calculated profiles are somewhat narrower than the observed profiles, in particular at the polarimeter. This can be attributed to multiple Coulomb scattering tails in the material along the beam line. Note that the polarised target itself presents a significant amount of material in the beam. In addition a veto counter with a thickness of 2 radiation lengths is installed at the beginning of the polarimeter decay section. The non-Gaussian tails of the scattering process in this material ($\approx 4X_0$ in total) have not been taken into account in the Monte Carlo simulations.

Despite the fact that the muon section optics was designed to be dispersion free, a definite correlation between individual muon momentum and vertical position was observed both at the polarised target and at the polarimeter. This correlation is also described by the Monte Carlo simulation and could be attributed to a dispersion in angle at the exit of the last vertical bend. The apparent dispersion (7 mm/% at the polarised target, – 4 mm/% at the entrance to MNP26) can be explained qualitatively and quantitatively by the presence of the absorber material (7.7 metres of Beryllium) in the first vertical bend of the muon section of the beam. Off-momentum muons can be scattered back into the beam acceptance if they are scattered towards the beam axis at the absorber. Thus high-momentum particles are kept preferentially if they are scattered upward and low-momentum particles if they are scattered downward, thereby leading to an angular distribution of accepted muons at the exit of the absorber which is biased in a momentum dependent way. As the angle of a muon at B4+5 is strongly correlated with its angle at the exit of B6, the scattering in the absorber leads to the observed correlation between angle and momentum of the muons. Since a vertical focus was planned in between the polarised target and the polarimeter section of the experiment, the net effect of this dispersion on the spot size remained well within the requirements specified by the experiment.

We conclude that the beam performance satisfies the requirements listed in section 2 and it agrees satisfactorily with the Monte Carlo simulations. This statement holds equally at the other beam momenta used by the Spin Muon Collaboration, namely – 100 and ± 208 GeV/c muon momenta.

7. SUMMARY AND CONCLUSIONS

The muon beam at the CERN Super Proton Synchrotron, operational since 1978 and recently upgraded for the Spin Muon Collaboration, has been described. Its observed performance fits the calculations and meets the specifications given by the experiment. At the typical beam momentum of 100 GeV/c the required flux of $4\ 10^7$ muons per SPS cycle is obtained using $3.5\ 10^{12}$ protons on primary target. The beam is almost fully contained within the polarised target of 5 cm diameter in the experimental hall. In the polarimeter section 70 metres downstream the RMS beam spot is smaller than 2.5 cm in each plane. The hard halo, defined as the rate in a 4x4 m^2 surface, outside a 50x50 cm^2 hole for the beam passage, is ≈6% at 100 GeV/c. At the highest beam momenta this hard halo is even as low as 4%. The measured longitudinal polarisation is (–82±6) %, in excellent agreement with Monte Carlo calculations.

Acknowledgements

It is a pleasure to thank the staff of the EA, PC and BI groups of CERN-SL Division for their continuous help and support in the installation and operation of the muon beam, in particular G. Caniac, B. Chauchaix, M. Clément, G. Dubail. G. Dubois, J. Hudry, W. Nägele and B. Tomat. The Beam Momentum Station was constructed and recently upgraded by the Beam Instrumentation group: we thank especially D. Brahy, K.D. Lohmann and E. Rossa for their invaluable contributions. K.D. Lohmann has also contributed to section 5 of this paper. The original design and performance of the muon beam owes much to the contributions of H.W. Atherton, C. Bovet, P. Grafström, D. Plane (CERN), F. Brasse, J. May (DESY), K. Brown (SLAC), R. Clifft (RHEL), L. Piemontese (Ferrara) and A. Staude (Munich). The present upgrade profited much from discussions with the Spin Muon Collaboration. We wish to mention in particular N. de Botton, F. Feinstein V. Hughes, T. Ketel, M. Lowe, G. Mallot, P. Shanahan and R. Voss. We also thank the collaboration for providing some of the data on the performance of the beam.

References

1) R. Clifft and N. Doble, Proposed design of a high-energy, high-intensity muon beam for the SPS North Experimental Area, CERN/SPSC/74-12 (CERN/Lab. II/EA/74-2).

2) M. Ballintijn et al., Measurement of the spin-dependent structure functions of the neutron and proton, Proposal to the SPSC, CERN/SPSC 88-47 (SPSC/P247).

3) O.C. Allkofer et al. (EMC), Electromagnetic interactions of muons, Proposal to the SPSC, CERN/SPSC 74-78 (SPSC/P18).

4) F. Ceradini et al. (BCDMS), Inclusive deep inelastic muon scattering, Proposal to the SPSC, CERN/SPSC 74-79 (SPSC/P19).

5) J. Beaufays at al. (NMC), Detailed measurements of structure functions from nucleons and nuclei, Proposal to the SPSC, CERN/SPSC/85-18 (SPSC/P210).

6) W. Kalbreier et al., Design principles of the target stations for the slow extracted proton beams of the SPS, CERN-Lab. II/BT/74-6.

7) P. Coet and N. Doble, An introduction to the design of high-energy charged particle beams, CERN/SPS/86-23 (EBS).

8) A.S. Carroll et al., Phys. Lett. B80 (1979) 319.
A.J. Malensek, Empirical formulae for thick target particle production, Fermilab FN-341/2941.000, 1981.

9) C. Bovet, Some properties of AG focusing, CERN SI/Note DL/68-24 , 1968.

10) J. Brahy and E. Rossa, Les hodoscopes du spectromètre M2, SPS/EBP/Note 77-5, 13/03/1977.
D. Brahy and E. Rossa, High-rate photomultiplier base and precise timing calibration, CERN-SPS/EA/78-11.

11) C.S. Wu et al., Phys. Rev. 105, 1413 (1957).
L.M. Lederman and M.J. Tannenbaum, Advances in Particle Physics, Vol. 1 (New York, N.Y., 1968), page 11.

12) See K.L. Brown et al., TRANSPORT, a computer program for designing charged particle beam transport systems, CERN 80-04 yellow report.

13) See C. Iselin , HALO, a computer program to calculate muon halo, CERN 74-17 yellow report.

14) See e.g. Review of Particle Properties, Phys. Rev. D45 (1992) and references therein.

15) P. Dreesen et al., Integrating wire chamber for beam tuning in the CERN SPS Experimental Area, CERN-SPS/EA 78-4.

16) P. Dreesen, Improvements on XWCA/XWCM integrator for use as beam intensity monitor, CERN SPS/EBP/Note 79-17.

17) The Spin Muon Collaboration, private communication. The authors wish to thank in particular N. de Botton, F. Feinstein and G.K. Mallot for their help.

18) B. Adeva et al. , A measurement of the spin-dependent structure function $g_1(x)$ of the deuteron, Phys. Lett. B302 (1993) 533.

19) B. Adeva et al., A high precision muon beam polarimeter, to be submitted to Nucl. Instr. and Methods.

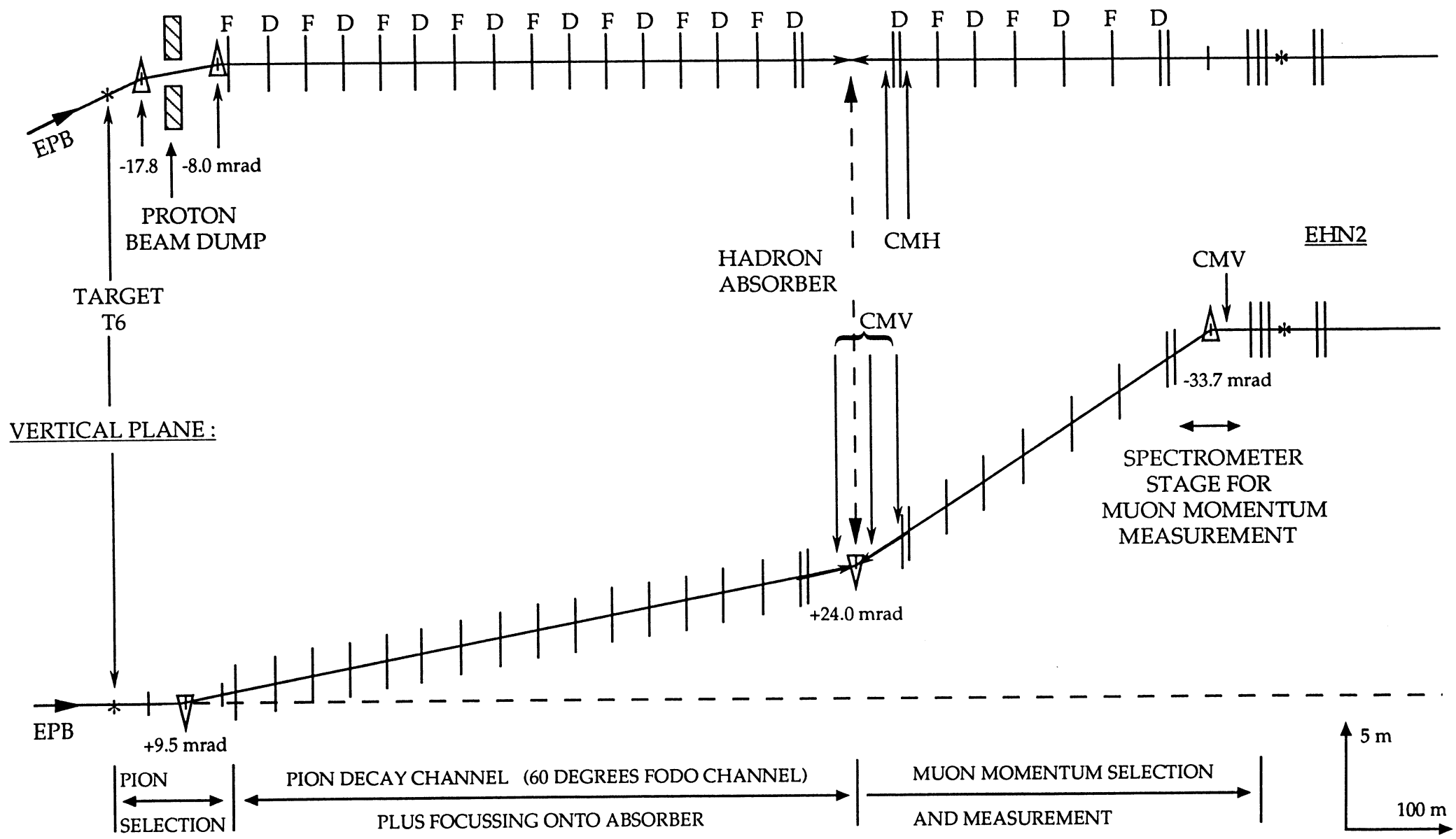

Figure 1: A schematic layout of the muon beam. The main functions of the different beam sections are indicated.

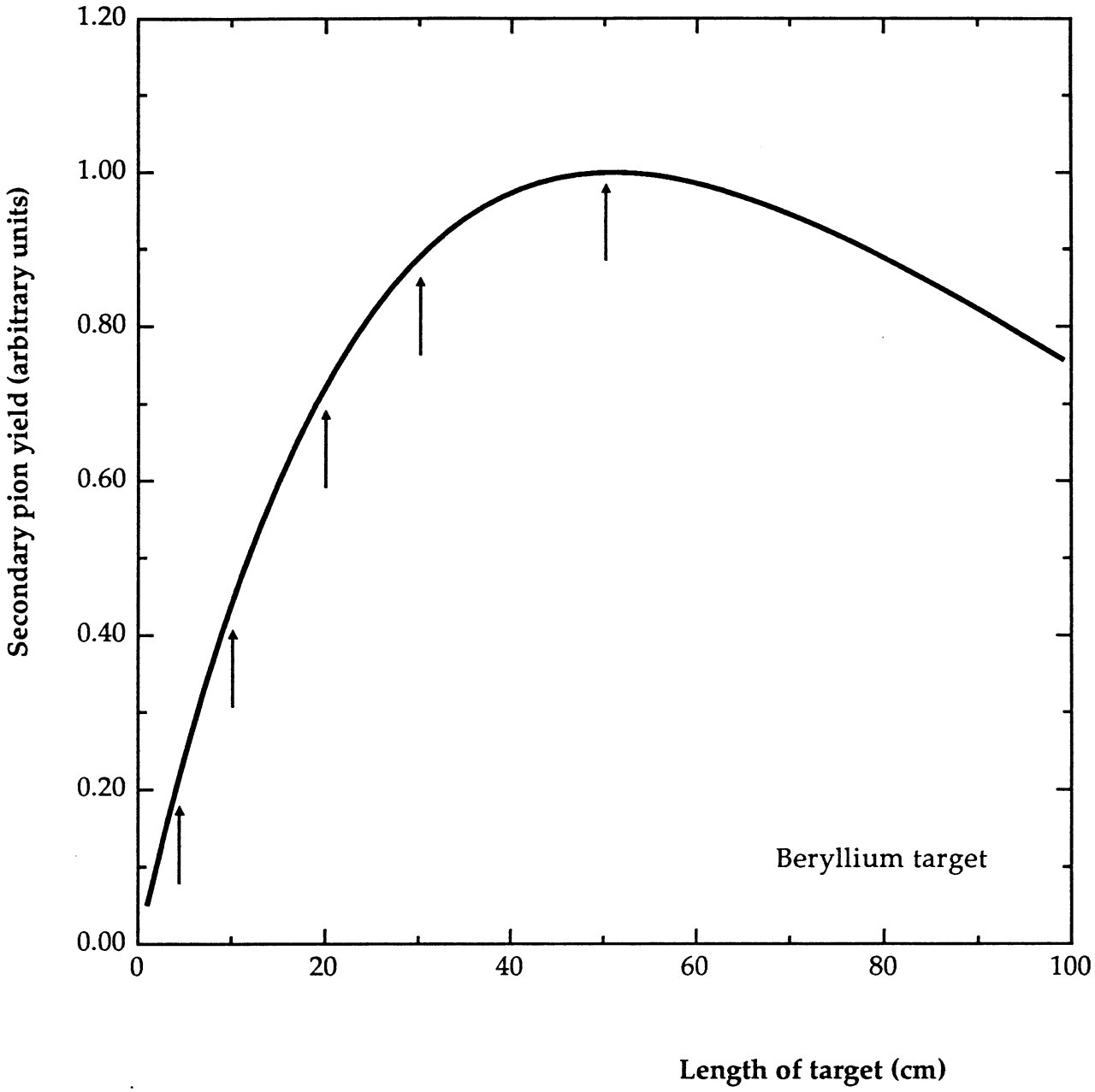

Figure 2 : The secondary pion yield from a Beryllium target as a function of its length. The arrows indicate the lengths of the available target heads.

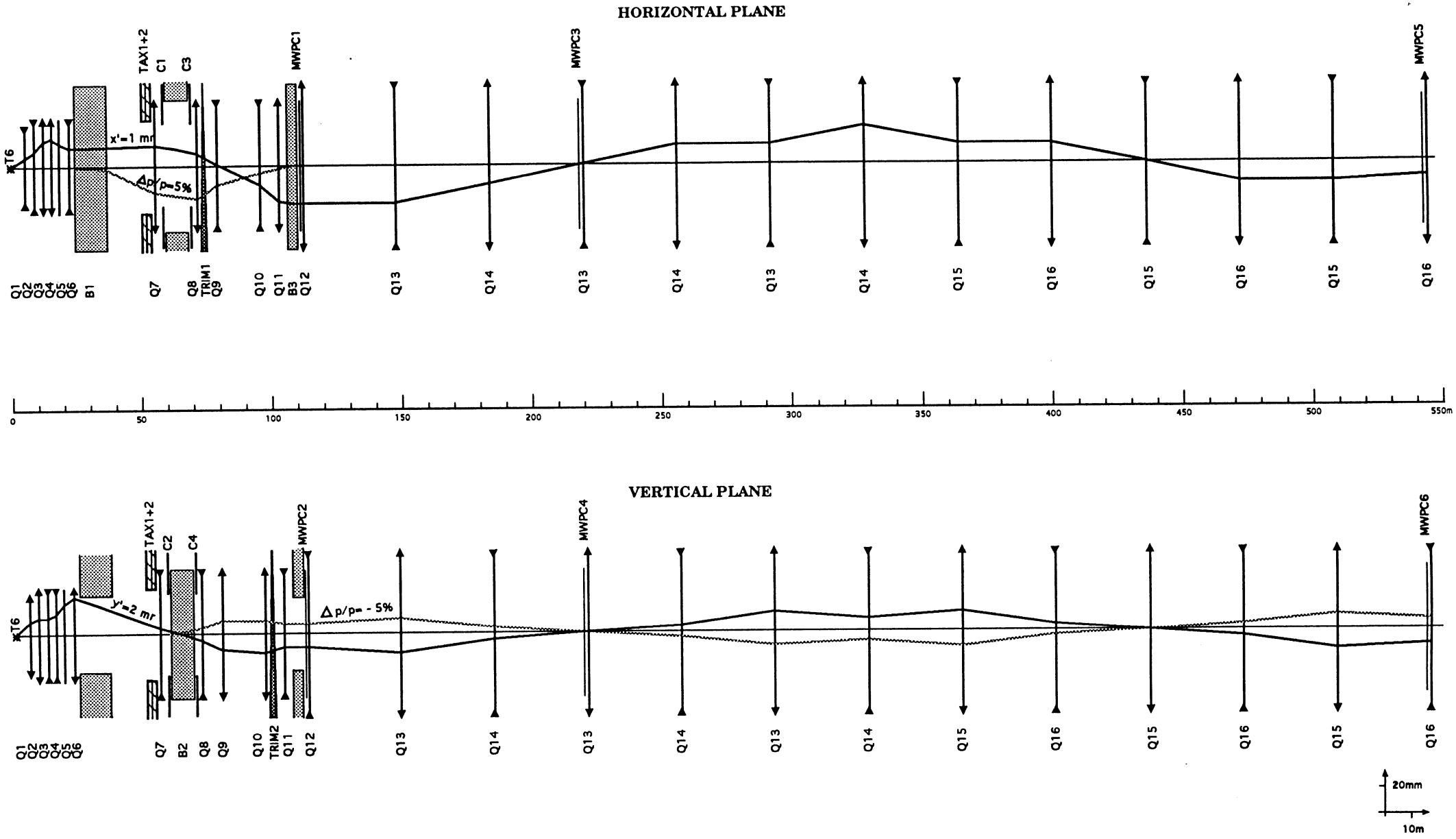

Figure 3 : The optics of the hadron section of the beam.

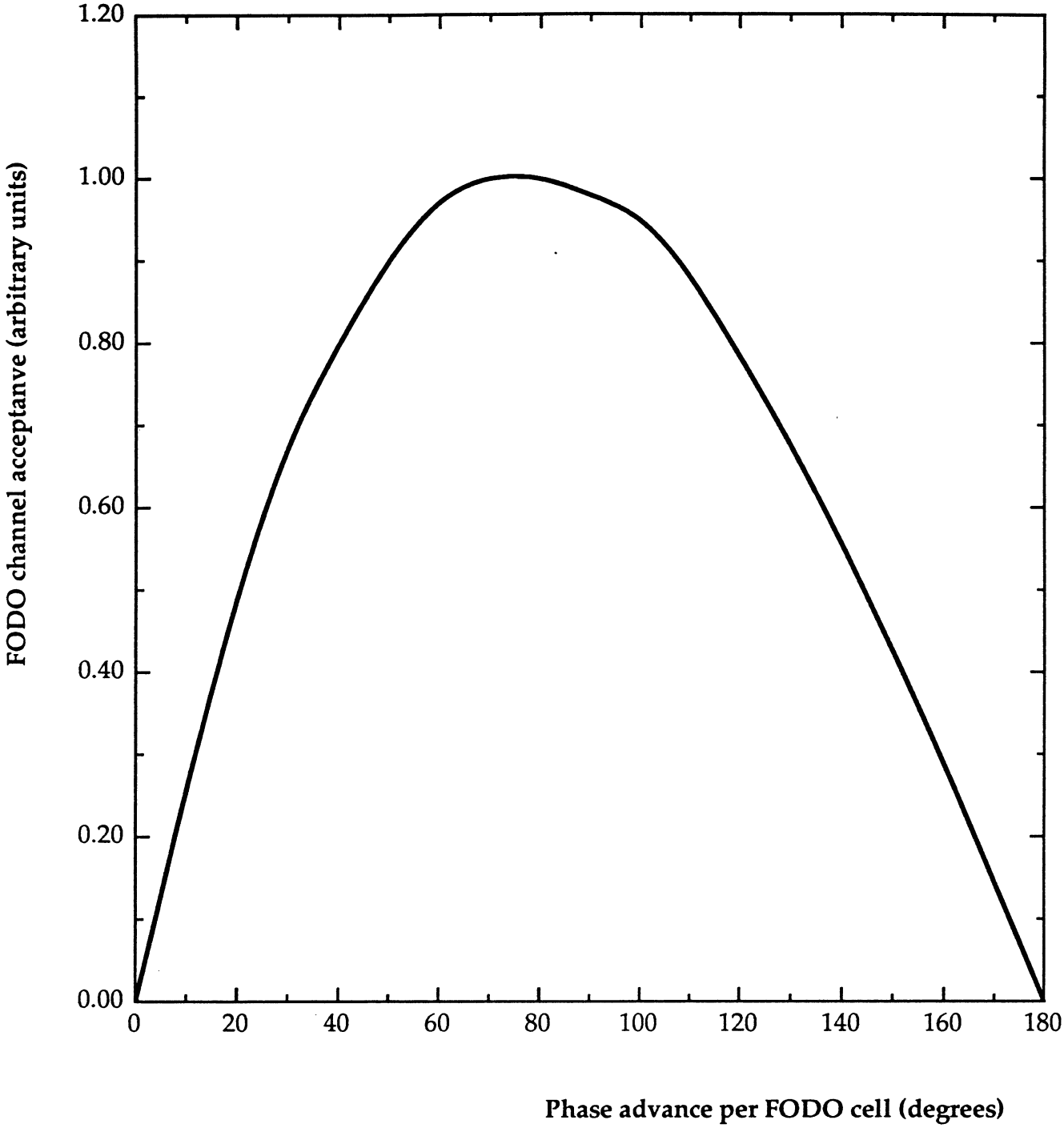

Figure 4 : The acceptance of a regular FODO channel (arbitrary units) versus the phase advance per cell (in degrees).

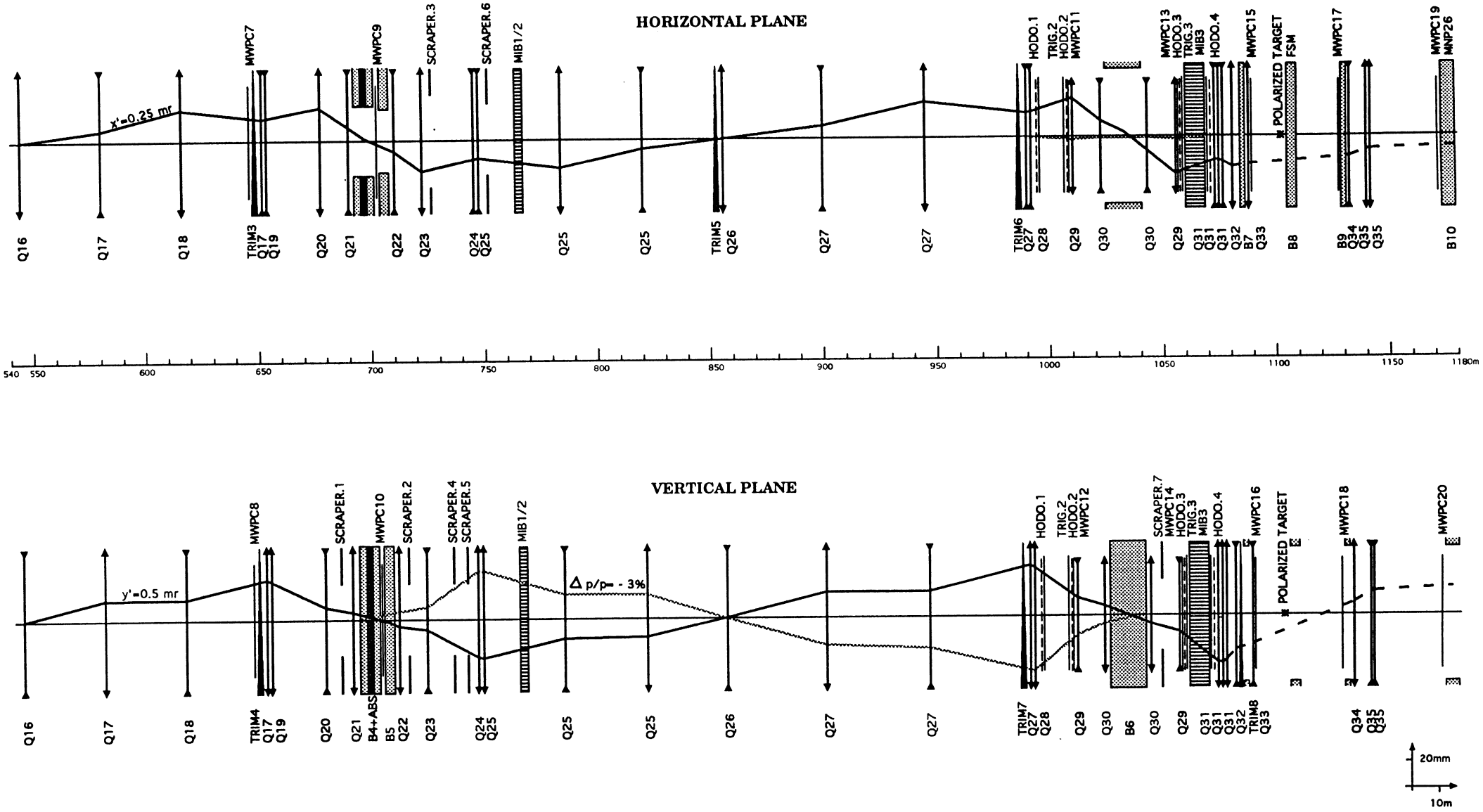

Figure 5 : The optics of the muon section of the beam.

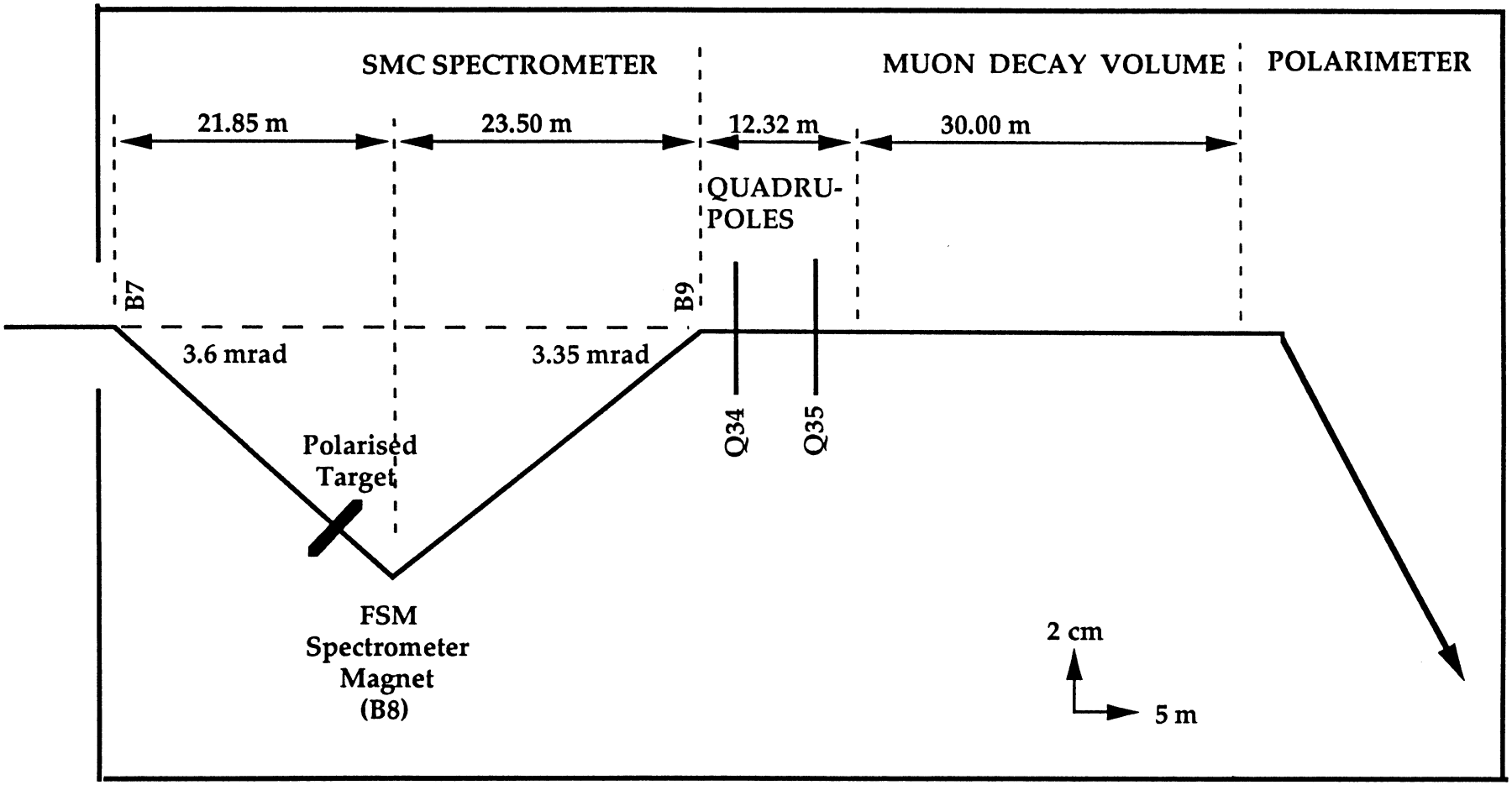

Experimental hall (not on scale)

Figure 6 : Schematic layout of the last section of the beam and the SMC experiment in the experimental hall EHN2.

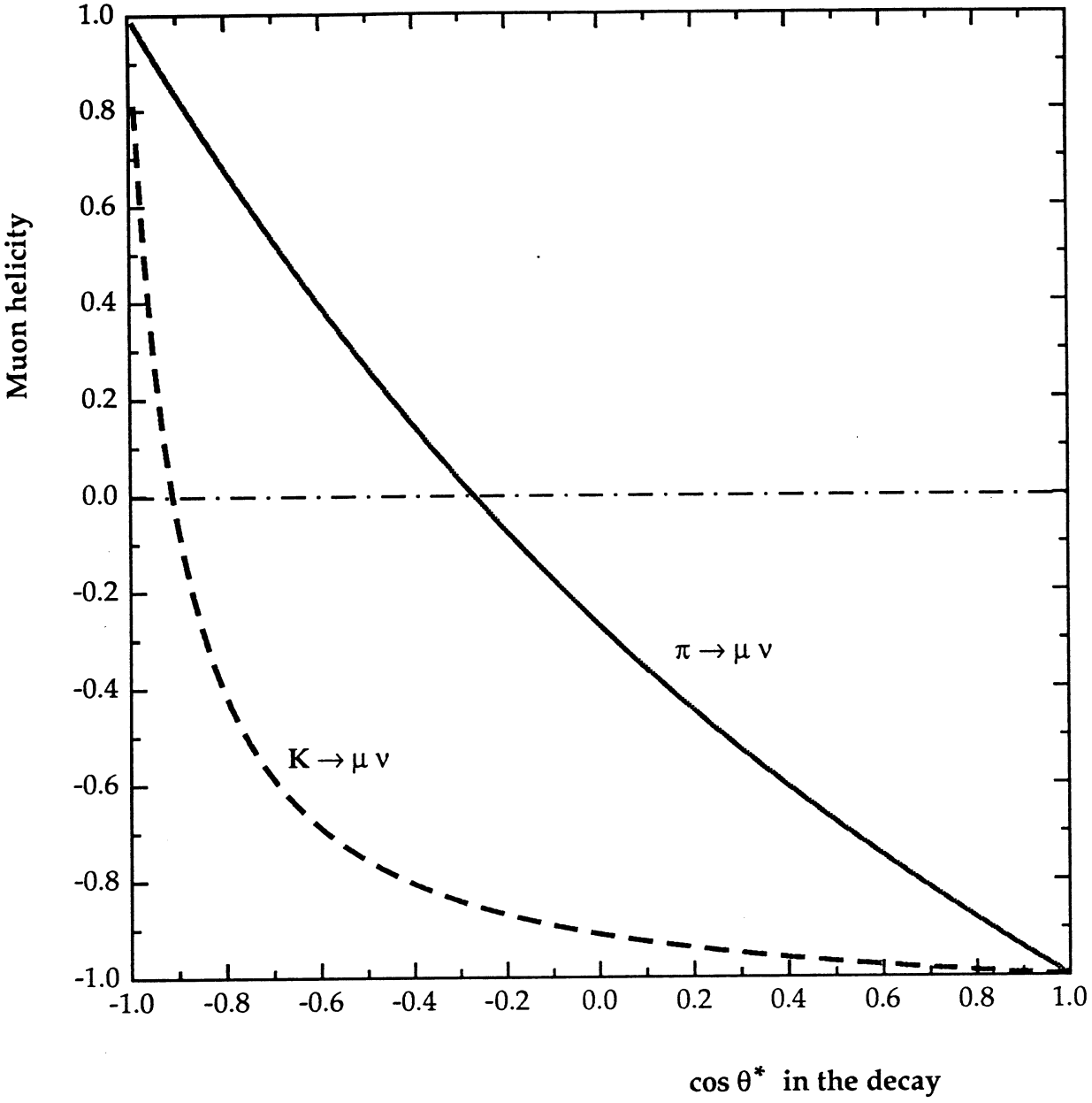

Figure 7 : The muon helicity versus the cos θ^* of the decay, both for pion and kaon decays

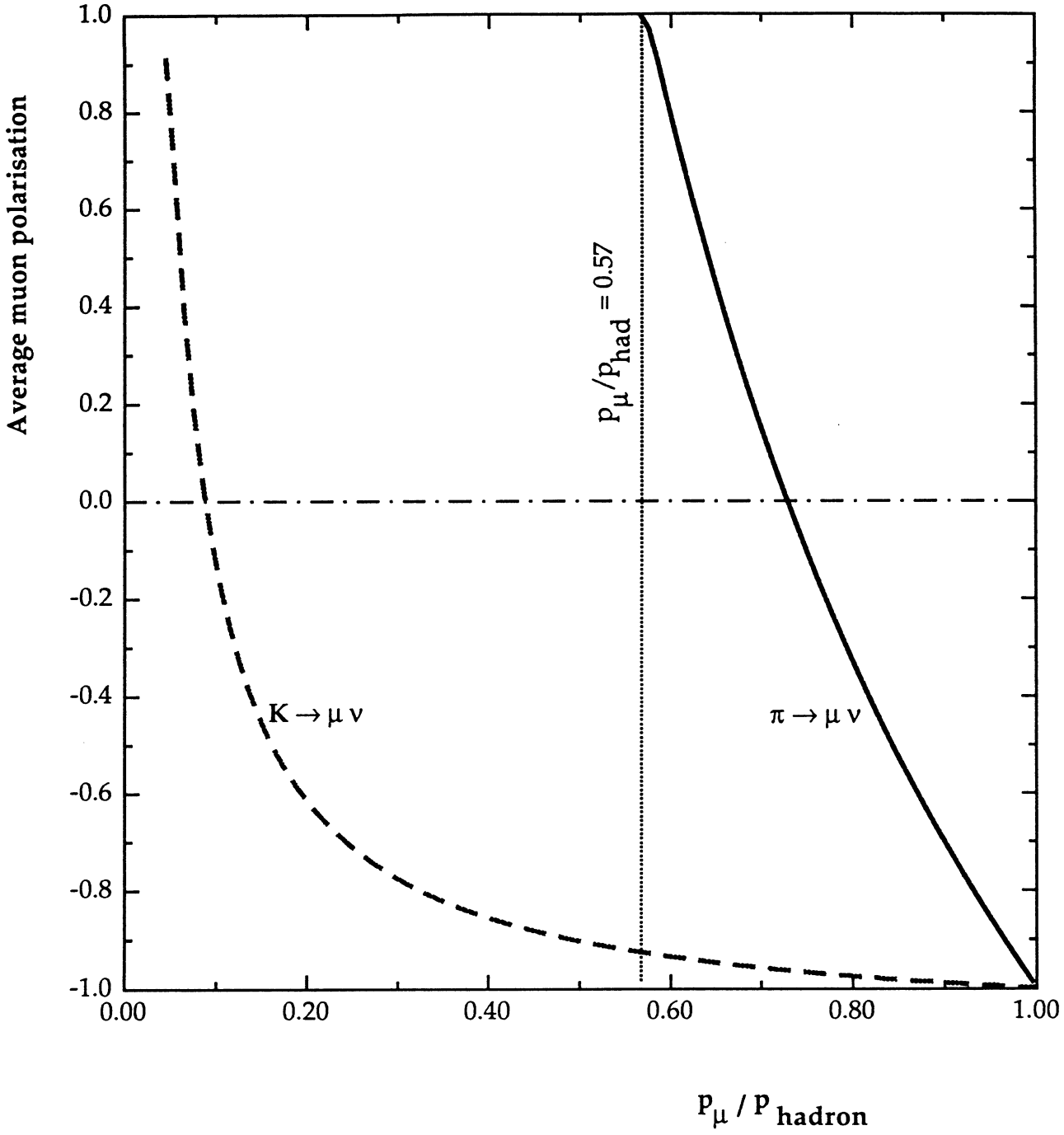

Figure 8 : The average muon polarisation as a function of the ratio p_μ / p_{hadron} of muon to parent hadron momentum. Plots are given separately for pion and kaon decays. Also indicated is the threshold for μ production from pion decays.

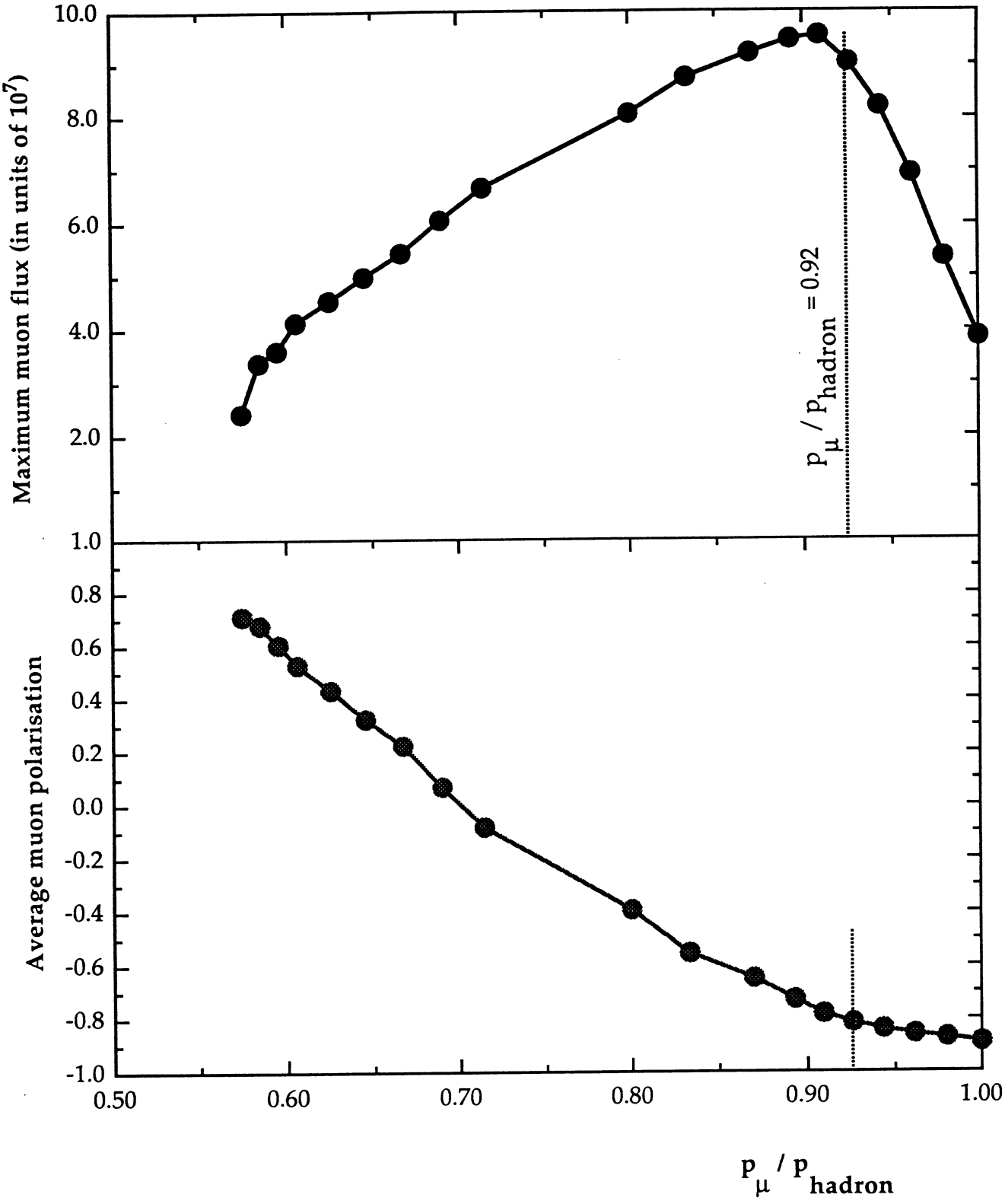

Figure 9 : The maximum achievable muon flux per 10^{12} protons interacting in the target and the average muon polarisation versus the ratio p_μ / p_{hadron}.

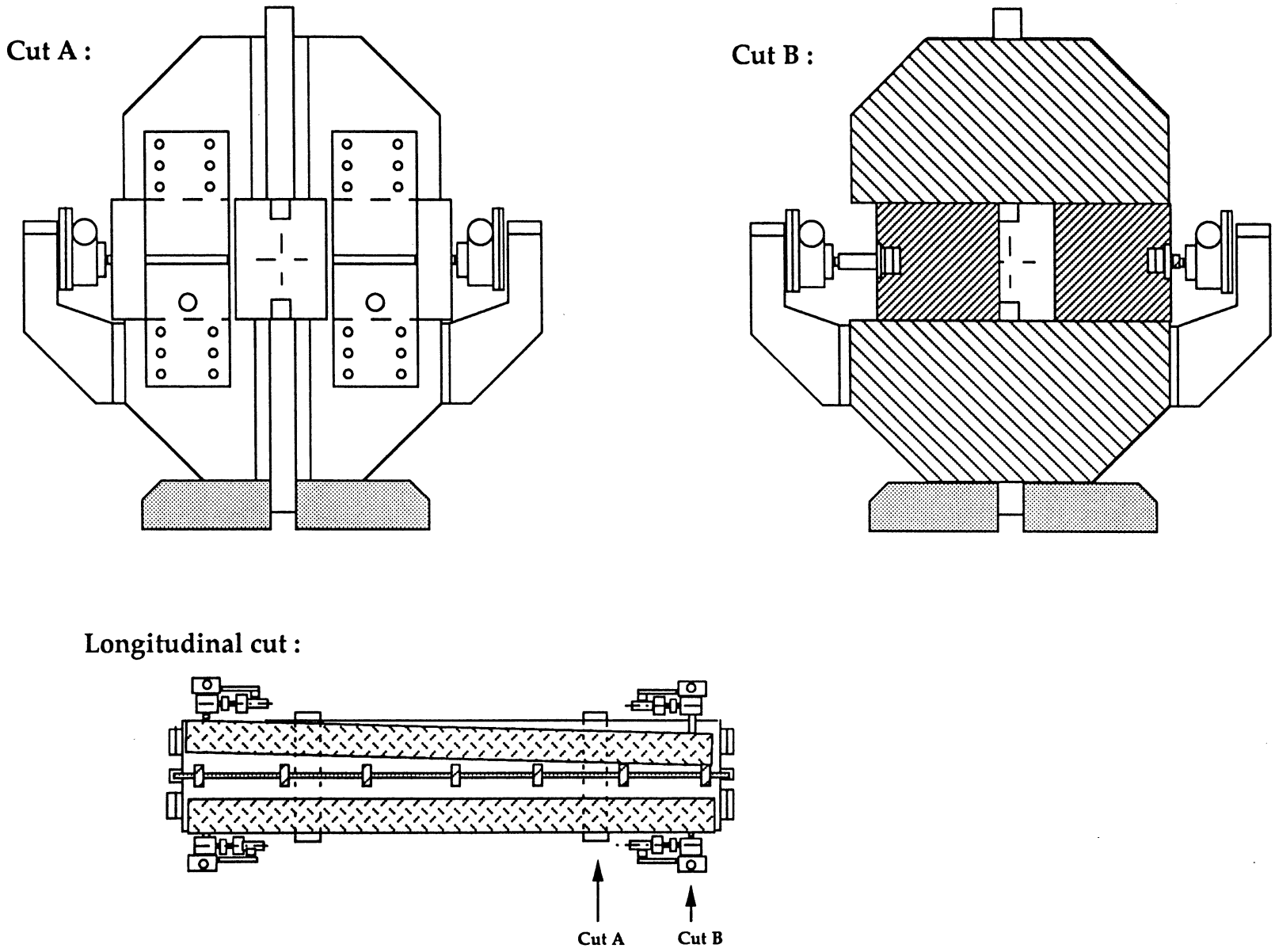

Figure 10 : A horizontal magnetic collimator (scraper). Two transverse cuts A and B are shown at the locations indicated in the longitudinal view, shown below.

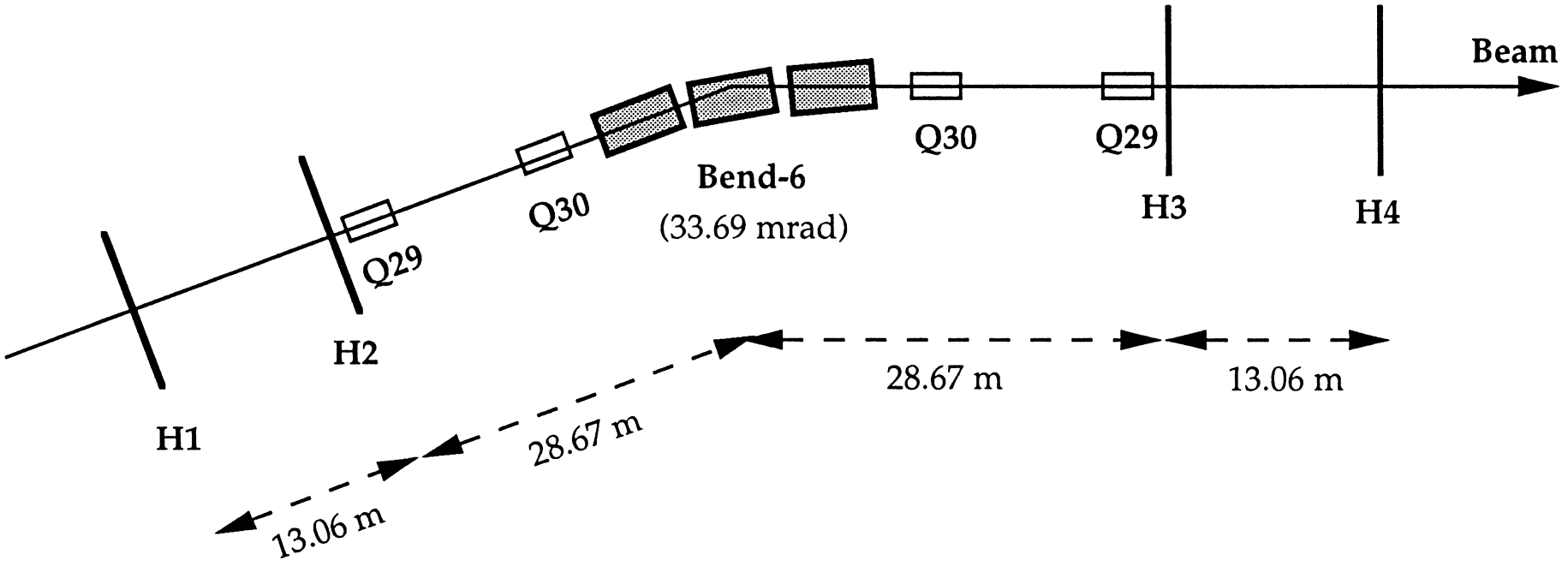

Figure 11 : Schematic layout of the Beam Momentum Station.

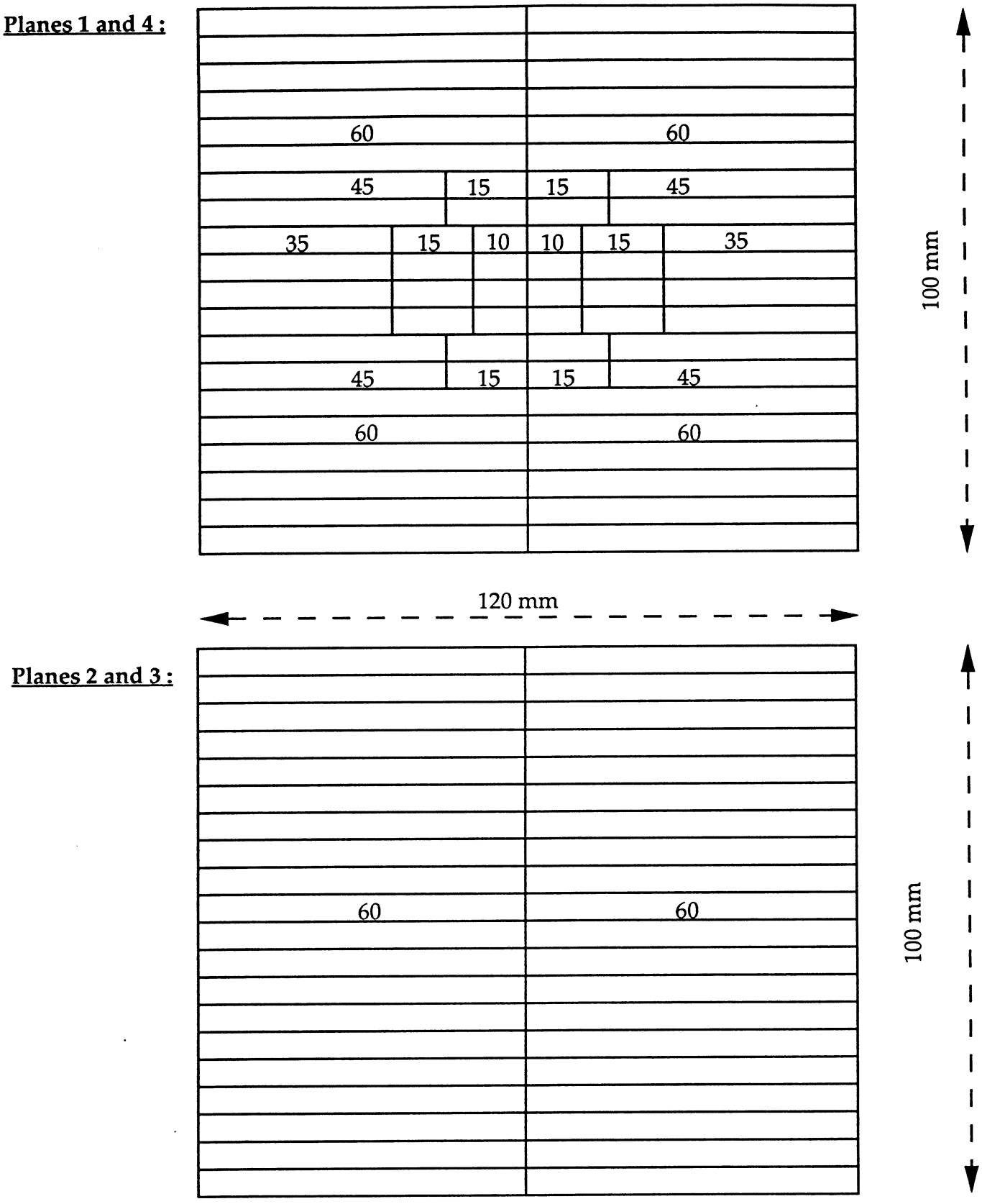

Figure 12 : The dimensions of the individual scintillator strips in the hodoscope planes.

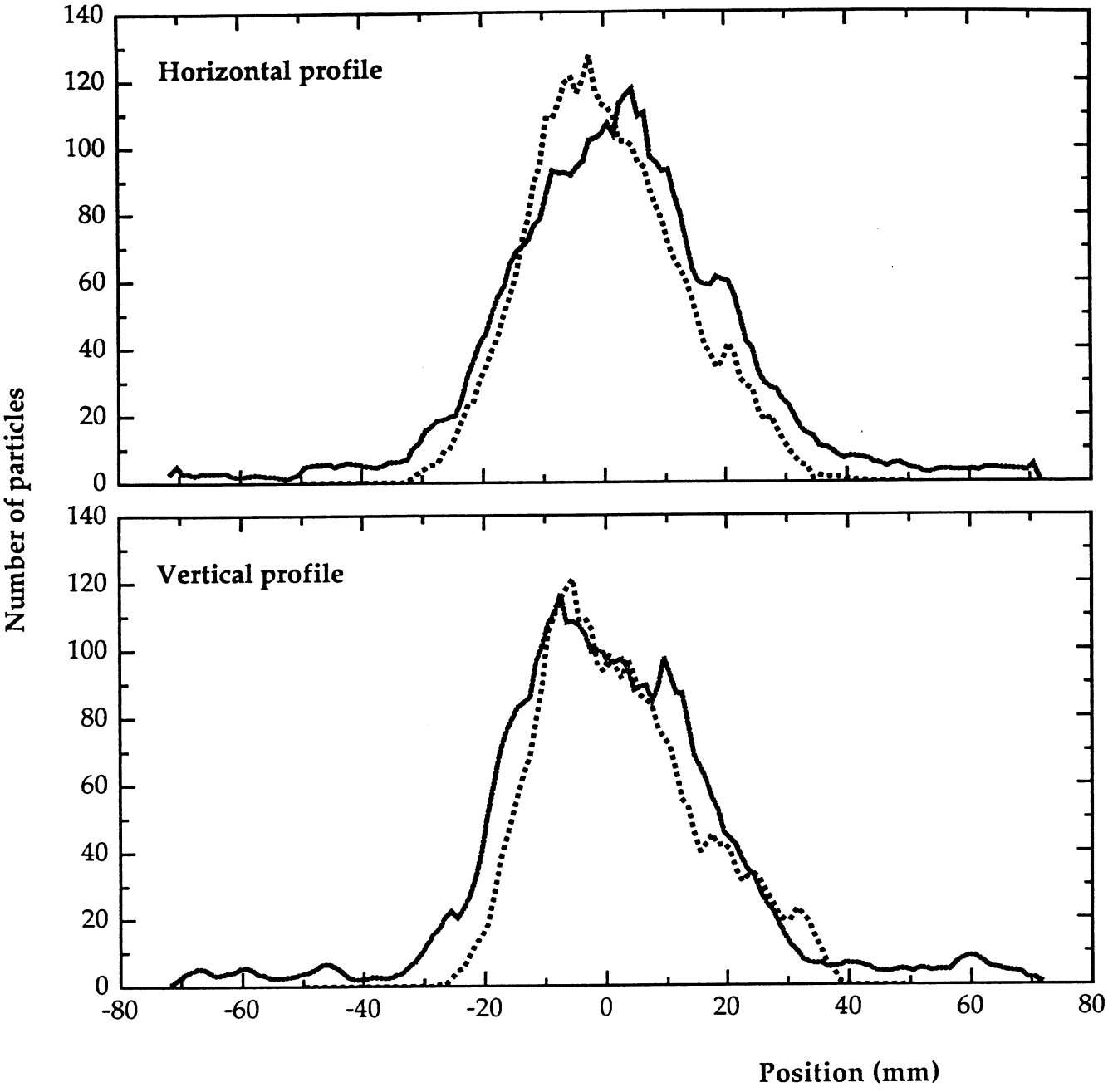

Figure 13 : The horizontal and vertical beam profiles at the polarised target.

The solid line shows data measured by the SMC collaboration.

The dotted line shows the Monte Carlo prediction for the profiles.

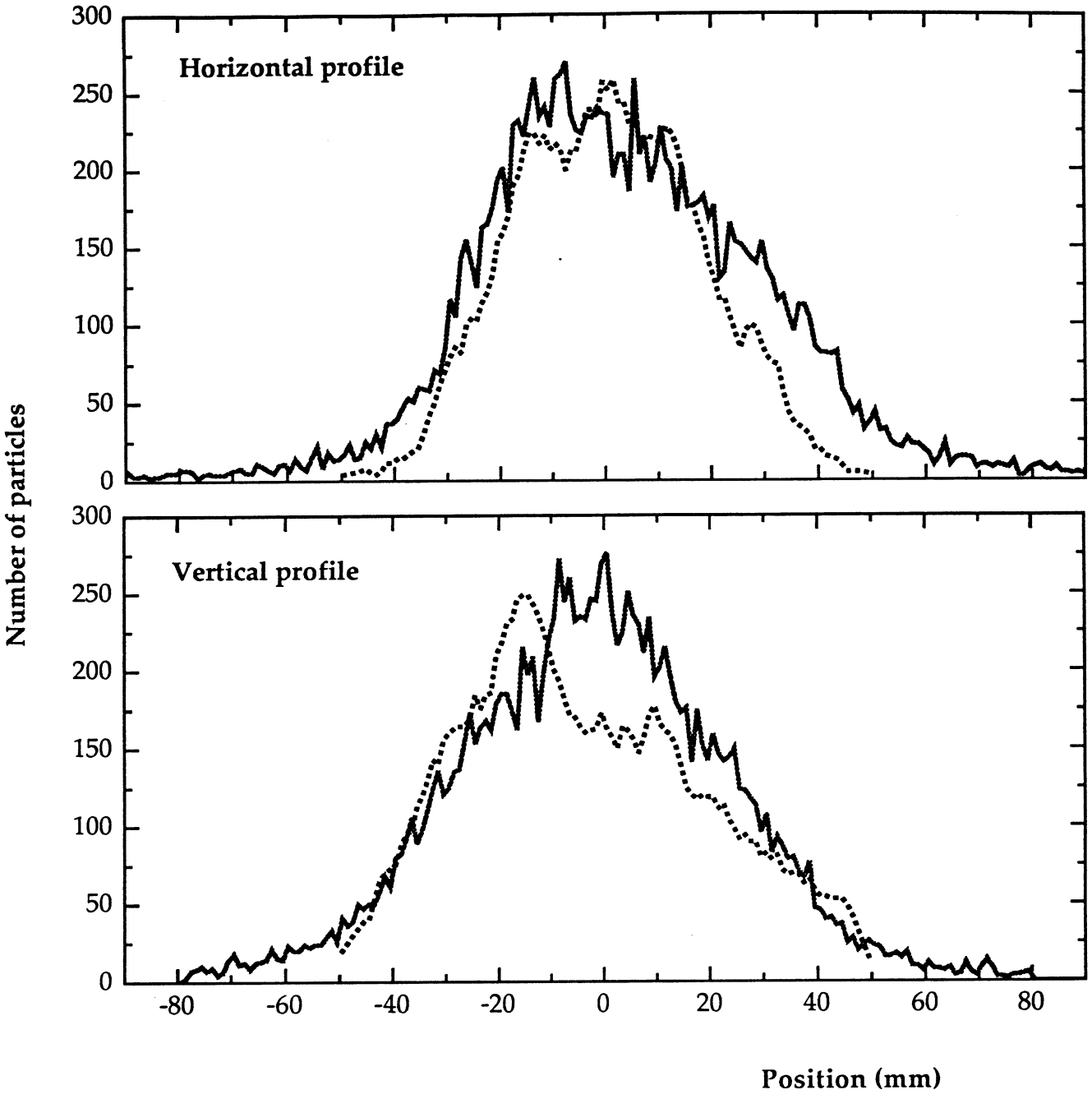

Figure 14 : The horizontal and vertical beam profiles at the polarimeter, i.e. 1.5 metres upstream of the entrance to the MNP26 spectrometer magnet.
The solid line shows the data measured by the SMC collaboration
The dotted line shows the Monte Carlo prediction for the profiles.